Experimental study of physical properties in the complex magnetic phase diagram of $Ce(Rh_{1-x}Ru_x)_3B_2$

St. Berger, A. Galatanu, G. Hilscher, H. Michor, Ch. Paul, and E. Bauer
Institut für Experimentalphysik Technische Universität Wien, A-1040 Wien, Austria

P. Rogl
Institut für Physikalische Chemie, Universität Wien, A-1090 Wien, Austria

M. Gómez-Berisso, P. Pedrazzini, and J. G. Sereni
Low Temperature Div., Centro Atomico Bariloche (CNEA), Conicet, 8400 S.C. de Bariloche, Argentina

J. P. Kappler
IPCM, Universite de Strasbourg, Strasbourg, France

A. Rogalev
European Synchrotron Radiation Facility, Boîte Postale 220, 38043 Grenoble, France

S. Matar, F. Weill, B. Chevalier, and J. Etourneau
ICMCB-CNRS UPR9048, Université Bordeaux I, Avenue du Dr. Albert Schweitzer, F-33608 Pessac Cedex, France

(Received 20 December 2000; revised manuscript received 9 April 2001; published 29 August 2001)

We report on a series of structural, magnetic, and thermodynamic measurements, a study of transport properties and x-ray absorption edge spectroscopy on $Ce(Rh_{1-x}Ru_x)_3B_2$. These investigations evidence that in addition to the already established ferromagnetic range for $x \leqslant 0.06$, a complex antiferromagnetic structure exists for concentrations $0.1 \leqslant x \leqslant 0.35$. The behavior in the latter regime is dominated by an extraordinary strong intersite coupling; however, the magnetic moments involved appear to be very small. At the phase boundary to the paramagnetic regime ($x \approx 0.4$), significant deviations from a Fermi-liquid behavior occur.

DOI: 10.1103/PhysRevB.64.134404 PACS number(s): 75.20.Hr, 75.30.Kz, 78.70.Dm, 71.10.Hf

I. INTRODUCTION

For almost two decades $CeRh_3B_2$ has attracted considerable interest because of its fascinating magnetic properties. Ferromagnetic ordering at $T_c \approx 115$ K (Ref. 1) labels this hexagonal ternary compound as the ferromagnet with the highest ordering temperature among Ce-based compounds with nonmagnetic ligands. The large value of this transition temperature and both the small effective magnetic moment [$\mu_{\text{eff}} \approx 1\ \mu_B$ (Refs. 2,3)] as well as the low saturation moment [$\mu_S \approx 0.38\ \mu_B$ (Refs. 1,4)] rules out de Gennes scaling, generally observed for well localized magnetic systems. The anomalously large Curie temperature has been attributed either to a strong exchange coupling between the Ce $4f$ and Ce $5d$ states,[5–7] or to the Ce f-Rh d hybridization.[4,8] A significant itinerant magnetic contribution of Rh, however, was never observed. This was concluded from both, polarized elastic neutron scattering[9] as well as from PES (Refs. 10,11) studies, revealing almost the same and small Rh $4d$ contribution to the density of states near to the Fermi energy [$N^{4d}_{\text{Rh}}(E_F) \approx 0.4$ states/(atom/eV) (Ref. 10)] for RRh_3B_2 with R=La, Ce, Pr. While $LaRh_3B_2$ is a Pauli paramagnet, the Pr-containing compound orders ferromagnetically below $T_c = 1.7$ K.

The significance of the Ce $4f$ and Ce $5d$ exchange in $CeRh_3B_2$ is obvious also from the non-negligible $5d$ magnetic moment ($\mu^{\text{tot}}_{5d} \approx -0.18\ \mu_B$), resulting in $\mu_{\text{Ce}} = \mu^{\text{tot}}_{4f} + \mu^{\text{tot}}_{5d} \approx 0.38\ \mu_B$,[9] in excellent agreement to the abovementioned magnetization data.[4] The $5d$ orbital contribution $\mu^L_{5d} = 0.16\ \mu_B$ signifies strong spin-orbit interaction.

Magnetic Compton scattering experiments[12] indicate that the Ce $5d$ spin moment is rather large, about $\mu^S_{5d} = -0.34\ \mu_B$ and parallel to the Ce $4f$ spin moment ($\mu^S_{4f} = -0.3\ \mu_B$). Hence, simple Kondo interactions seem to be of minor importance. Triggered by this unusually high ferromagnetic ordering temperature, substitution variants concerning all three atomic species have attracted high interest to reveal the physical nature of the driving force and the particular type of the magnetic interaction.

The substitution of Rh/Ru caused the most dramatic suppression of ferromagnetic order, at a ratio of 6 K/at % Ru.[4,13,14] Magnetic measurements indicated the absence of ferromagnetic order for $x > 0.1$ but hints to a magnetically ordered state are provided by susceptibility and resistivity data in the case of $x = 0.2$.[13] A similar behavior was observed by Shaheen *et al.*[4] for $0.16 \leqslant x \leqslant 0.23$, related either to antiferromagnetism or spin fluctuation effects. Compounds in the concentration range $0.7 \leqslant x \leqslant 1$ are superconducting. $T_{\text{SC}} = 0.7$ K for $CeRu_3B_2$ and decreases upon the Ru/Rh substitution towards zero.[2,13]

A recently started reinvestigation of the entire system indeed revealed a more sophisticated physical behavior not

recognized earlier. On the basis of preliminary studies of magnetic, transport, and thermodynamic quantities, a complex magnetic phase region was established for $0.1 \leqslant x \leqslant 0.4$. Consequently further investigations were required and the detailed analysis of the relevant physical quantities constitute the subject of the present paper. Subsets of these results were already published at various international conferences.[15,16]

II. EXPERIMENTAL

A series of 20 alloys within the concentration range $0 \leqslant x \leqslant 0.6$ were prepared by argon arc melting on a water cooled copper hearth. Starting materials were ingots of 99.9% pure Ce of Auer Remy, D and compacts of proper blends of powders of 99.8 % pure crystalline B (United Chemicals, USA) and 99.9 % Ru, Rh from Ögussa, A. To ensure homogeneity, the alloy buttons were turned over and remelted several times. Prior to final melting the reguli were broken and outer parts arranged to become inner parts. With such a procedure single phase material was achieved, which from Camebax SX50 EMPA spot and line scan analyses proved a remarkable homogeneity: correspondence of the actual composition for all elements with the nominal composition was in all cases within 1 at. % (it shall be noted that also the boron concentration was directly measured in EMPA). X-ray analyses were performed on finely ground powders either at room temperature using Guinier film and image plate techniques or down to He temperatures in a D500 diffractometer with the flat specimen mounted in an Oxford He-flow cryostat. Electron diffraction (TEM) was performed at 200 keV on a JEOL 2000 FX.

The electrical resistivity and magnetoresistivity of bar shaped samples were measured using a four probe dc method in the temperature range from about 0.5 K to room temperature and fields up to 12 T. A SQUID magnetometer served for the determination of the magnetization from 2 up to 300 K in fields up to 6 T. Specific heat measurements on samples of about 1–2 g were performed in two calorimeters at temperatures ranging from 0.4 up to 25 K and from 1.5 up to 120 K by means of a quasiadiabatic step heating technique. Ce $L_{\mathrm{II,III}}$ x-ray absorption spectroscopy (XAS) measurements were carried out at the ESRF beam-line ID12A in the total fluorescence detection mode.

III. RESULTS AND DISCUSSION

A. Crystal structure and electronic band structure calculations

X-ray powder analysis in all cases revealed isotypism with the ordered $CaCu_5$ type structure ($CeCo_3B_2$). No superstructure lines were observed, as a proof for random distribution of Rh and Ru atoms at the $3(g)$ site of the structure (space group: $P6/mmm$). The $CaCu_5$ type lattice geometry and particularly the absence of superstructure were inferred from TEM exposures for $x=0.2$ and $x=0.4$ (Fig. 1).

Figure 2 shows the composition dependency of the unit cell parameters at room temperature. It is interesting to note

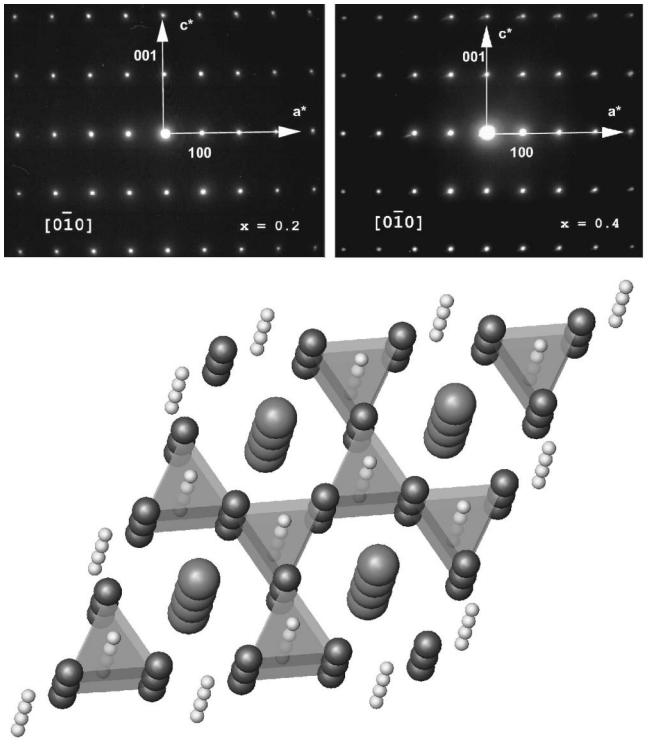

FIG. 1. Crystal structure of $Ce(Rh_{1-x}Ru_x)_3B_2$ and reciprocal lattice planes for $x=0.2,0.4$.

that the major variation of the unit cell parameters occurs for $0 \leqslant x \leqslant 0.4$, yielding a small maximum in a and a slight minimum in c around $x \approx 0.2$. While the volume contraction amounts to only 1.3%, the changes in a and c are as large as 2 and 4 %, respectively. The very similar dependence for the homologous system $La(Rh_{1-x}Ru_x)_3B_2$,[17] invokes the conclusion that the major driving force for this anisotropic dependency of the unit cell dimensions is to be found in the Rh/Ru substitution mechanism. As a consequence, the gradual increase of the cerium valency in the Rh-rich concentration range seems to be of minor influence in this range of concentration (see discussion below).

The temperature dependence of the lattice parameters normalized to the 300 K values is monitored in Fig. 3 for the temperature region 3.5 to 300 K. In this graph, our measurements for $x=0.2$ and $x=0.4$ are compared with data from literature for $CeRh_3B_2$.[18] The highly anisotropic variation of the unit cell dimensions of $CeRh_3B_2$ reveals magnetostriction effects due to the ferromagnetic state below $T_C = 115$ K. The dilatation in the a direction on cooling may be a direct hint of crystal field effects, absent for $LaRh_3B_2$. The Rh/Ru substitution diminishes this effect significantly to values which for $x=0.4$ compare with nonmagnetic $LaRh_3B_2$. The observed decrease of the temperature-dependent anisotropy in the Ce series may thus be interpreted as a gradual loss of magnetism. A corresponding discussion on magnetic properties will be carried out below. As a direct measure for the rare earth atoms distance, the c parameters are extremely small and in fact they are significantly shorter than interatomic distances in α cerium even under pressure.[19] Despite

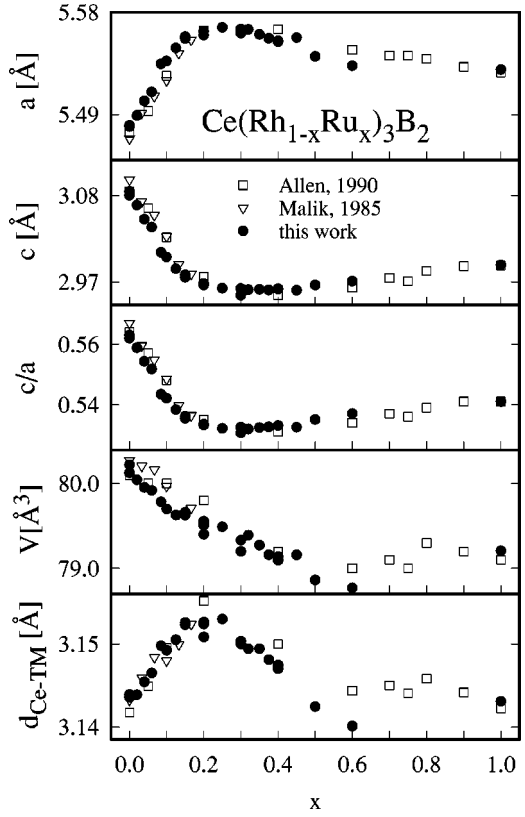

FIG. 2. Concentration-dependent lattice constants *a*, *c*, unit cell volume *V*, and cerium–transition-metal distance $d_{\text{Ce-Rh,Ru}}$ of $Ce(Rh_{1-x}Ru_x)_3B_2$.

this extremely close Ce-Ce distance, the Rh/Ru substitution as well as the temperature dependence tend to further reduce the *c* axis.

The electronic properties of CeT_3B_2 (T=Ru,Rh,Pd) have been self-consistently calculated within the local spin density functional theory (DFT) using the augmented spherical wave (ASW) method[20] in a scalar relativistic implementation.[21]

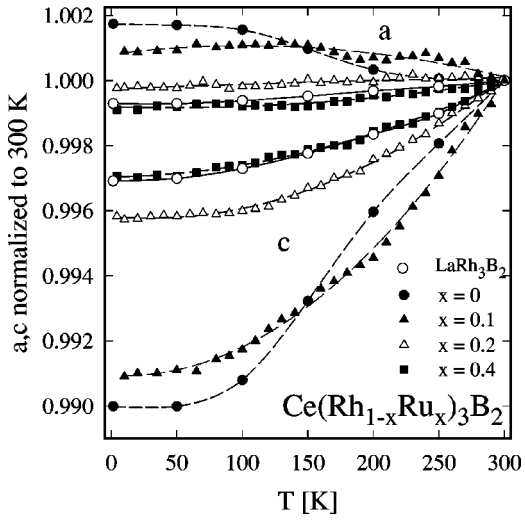

FIG. 3. Temperature-dependent lattice constants for various concentrations of $Ce(Rh_{1-x}Ru_x)_3B_2$ and $LaRh_3B_2$.

The effects of exchange and correlation are treated within the local spin density approximation (LSDA) using the parametrization scheme of von Barth and Hedin[22] and Janak.[23] All valence electrons, including Ce($4f$) were treated as band states. In the minimal ASW basis set,[20] we chose the outermost shells to represent the valence states and the matrix elements were constructed using partial waves up to $l_{\max}+1=4$ for Ce, $l_{\max}+1=3$ for T and $l_{\max}+1=2$ for B. In addition to the DFT, the ASW uses the atomic sphere approximation (ASA) which assumes overlapping spheres centered on the atomic sites where the potential has a spherical symmetry. The volume of all the spheres is made equal to the cell volume. From this the choice of the atomic radii is not unique and makes any discussion of charge transfers tentative. Rather, it can be argued that the bonding in these systems appears to be mainly driven by hybridization effects than by charge transfer.

Figure 4 summarizes the density of states (DOS) as well as the crystal orbital overlap populations (COOP's) for the compounds $CeRu_3B_2$, $CeRh_3B_2$, and for hypothetical $CePd_3B_2$. The same energy window is considered for all three compounds and the Fermi level (E_F) is taken as zero energy. In all three cases the cerium DOS shows a large peak around E_F mainly due to the $4f$ states as well as a contribution from itinerant Ce ($5d$) states below E_F which play a dominant role in bonding with the transition metal states. As the low lying Ce($4f$)-DOS is cut by the Fermi level the major part of the *f* bands remain unoccupied and are centered above E_F. The Ce($4f$) band width does not significantly alter from Ru to Pd, but transition metal DOS centered around $-1--5$ eV for Ru naturally lowers in energy with respect to the Fermi energy with increasing number of electrons to $-2--6$ eV for Rh and to $-3--7$ eV for Pd, respectively.

Considering the COOP curves we immediately recognize the high level of antibonding states at E_F for $CePd_3B_2$ eventually explaining the observed instability of this structure type in the Ce-Pd-B system. Interestingly Ce-Ru bonding seems to be significantly stronger than for Ce-Rh and Ce-Pd. This could in fact explain the decaying magnetism within $Ce(Rh_{1-x}Ru_x)_3B_2$ with increasing x due to increasing Ce-Ru hybridization. Preliminary spin polarized calculations actually show this trend. While the Ce-Ce overlap is strongest for the Pd-containing hypothetical compound it is interesting to note that Ce-B bonds within the boron-centered tetrakaidekahedral unit $[Ce_3T_6]B$ are becoming stronger along the series Ru-Rh-Pd, but transition metal-boron interactions within the characteristic triangular $[T_6]B$ prisms significantly decrease from Ru to Rh becoming strongly antibonding for Pd.

However, when assuming a continuous change of hybridization when proceeding from $CeRh_3B_2$ to $CeRu_3B_2$, physical properties may generally not directly follow this trend, since the lattice parameters, and thus interactions between the various atoms, change in a non-uniform way (compare Fig. 2).

B. Magnetic properties

The magnetic behavior within the series $Ce(Rh_{1-x}Ru_x)_3B_2$ is summarized in Figs. 5(a), 5(b), and

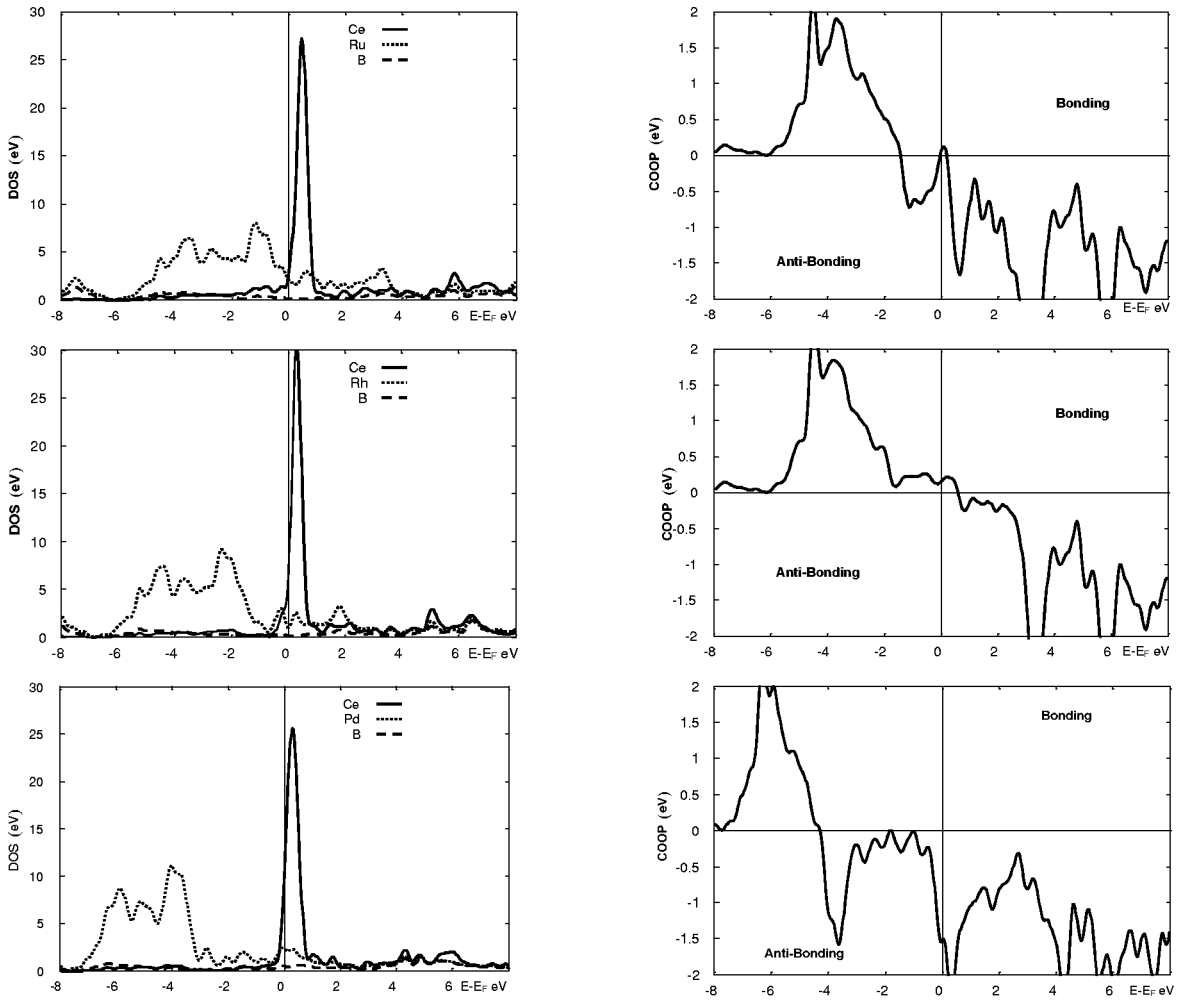

FIG. 4. Electronic structure of CeT_3B_2, T=Ru, Rh, Pd; density of states (DOS) (left); crystal orbital overlap population (COOP) (right).

6(a), 6(b). Figure 5(a) displays the magnetization M vs temperature for $0 \leqslant x \leqslant 0.125$. From the corresponding Arrott plots in Fig. 6(b) spontaneous magnetization can only be attributed to Ru concentrations up to $x=0.06$. The absence of spontaneous magnetization for $x \geqslant 0.085$ locates the decay of ferromagnetism at a somewhat lower concentration than earlier reported.[13,4,14] Ferromagnetic order with moments in the basal plane was established from neutron diffraction experiments for $CeRh_3B_2$ exhibiting an ordered Ce moment of $\mu_{\mathrm{ord}} \approx 0.40\ \mu_B$.[9] The spontaneously ordered magnetic moment for $CeRh_3B_2$ extrapolated from M vs H data to $H \rightarrow 0$ amounts to about 0.28 μ_B/f.u. and reduces upon Rh/Ru substitution to 0.26, 0.21, and 0.14 for $x=0.02, 0.04, 0.06$, respectively [compare Fig. 6(a)]. The strong nonlinear decrease extrapolates further to a vanishing spontaneous magnetization for $x \approx 0.08$ in good agreement with the Arrott plots in Fig. 6. Although the deduced spontaneous magnetic moments are smaller than those reported by Malik *et al.*,[14] Kasaya *et al.*,[24] and Allen *et al.*,[13] they directly correspond as polycrystalline materials to the moment contribution from the basal plane only[9] at least in the case of parent $CeRh_3B_2$.

For higher concentrations in x, M/H is plotted as a function of temperature in an external field of 1 T [Fig. 5(b)]. The overall shape shows a distinct variation with respect to the ferromagnetic regime $x \leqslant 0.08$. As a prominent feature, concentration-dependent local maxima are seen, slowly growing up to 65 K at $x=0.2$. However, above about $x=0.35$ such a phase boundary is not detectable any more.

Elastic neutron scattering experiments performed at the high flux spallation source of the PSI-Villigen, Switzerland on 11^B based material from the complex phase region with the highest ordering temperature did not reveal any significant scattering amplitude as a difference between the paramagnetic and the magnetically ordered state. Thus attempts to derive the nature of the magnetic order failed. This indicates an extreme weakness of the ordered moments ($\mu_{\mathrm{ord}} < 0.2-0.3\ \mu_B$), essentially confirming the low moments observed in magnetization measurements reported above.

For an evaluation of the temperature variation of the susceptibility, a modified Curie Weiss law was applied. Least squares fits for temperatures $T>100$ K yield the paramagnetic Curie temperature θ_p, the effective magnetic moment μ_{eff}, and a temperature independent contribution χ_0, the latter ranging between 0.5 and $1.5\times10^{-3}\mu_B$/T. A plot of θ_p and μ_{eff} vs the Ru concentration is summarized in Fig. 7. Following the variation of θ_p, there is fine agreement with the composition where θ_p changes sign, and the simulta-

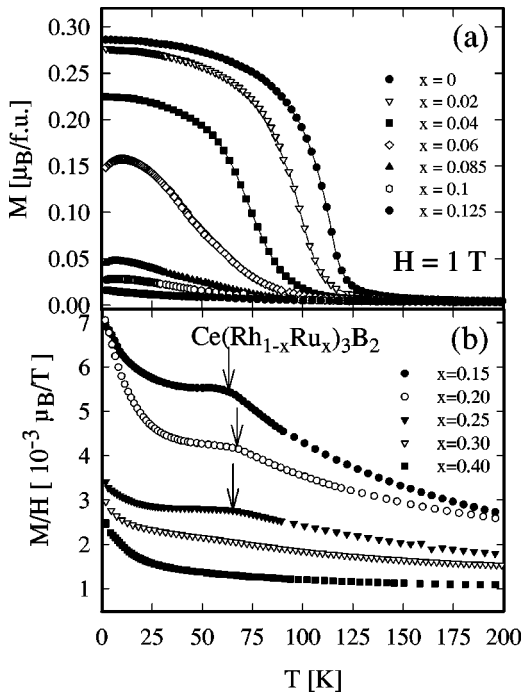

FIG. 5. Temperature-dependent magnetization of $Ce(Rh_{1-x}Ru_x)_3B_2$, (a) $0 \leqslant x \leqslant 0.125$ and (b) $0.15 \leqslant x < 0.4$ measured at $\mu_0 H = 1$ T.

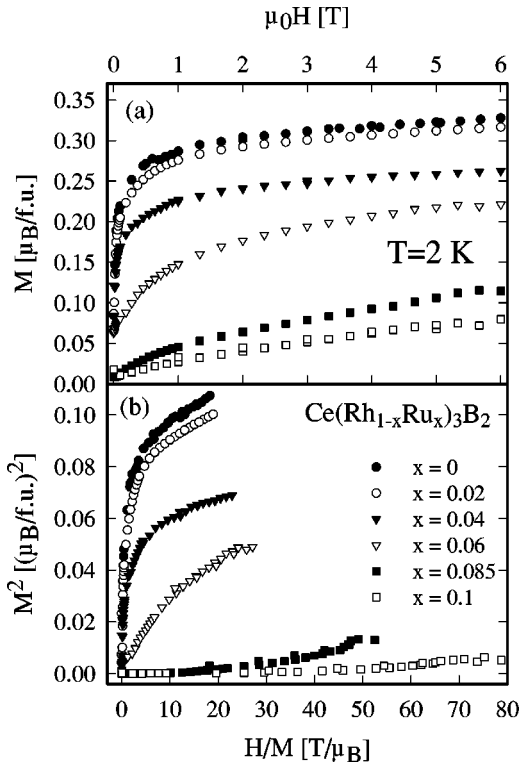

FIG. 6. (a) Isothermal magnetization at $T = 2$ K for various concentrations of $Ce(Rh_{1-x}Ru_x)_3B_2$. (b) Arrot plots of $Ce(Rh_{1-x}Ru_x)_3B_2$, $0.0 \leqslant x < 0.1$, derived at $T = 2$ K.

neous change in the magnetic structure, which is no longer ferromagnetic. The fairly large negative θ_p values between $0.15 \leqslant x \leqslant 0.25$ are in agreement with the local maxima in the temperature dependent susceptibility which are both suggestive of antiferromagnetic order in this concentration range. The reduction of the absolute values of θ_p towards $x = 0.35$ is concomitant with the loss of distinct features in the susceptibility curves and questions the applicability of the used modified Curie Weiss law in this region. The effective magnetic moment μ_{eff} rises up to a maximum value at $x = 0.15$ from where it drops and extrapolates to zero for $x \approx 0.4$. The unexpected rise of μ_{eff} may be due to a growing localization of the Ce ion moments caused by the initial increase of the Ce-TM distance (see Fig. 2). A similar increase of the effective magnetic moment is observed when cerium is diluted with larger atoms such as lanthanum.[4] The drop of μ_{eff} for concentrations $x > 0.15$, however, follows the reduction of available electrons and the simultaneous increase of hybridization driven by the Rh/Ru substitution, in line with the again decreasing Ce-TM distances for $x > 0.2$ (compare Fig. 2).

Attempts were made to analyze the paramagnetic susceptibility well above the ordering temperature in terms of appropriate crystal field contributions and where interactions were accounted for by molecular field constants.[15] Such a procedure reveals for $x = 0.2$ a $\pm|1/2\rangle$ ground state doublet with a first excited $\pm|5/2\rangle$ level between 500–800 K. The uppermost level $\pm|3/2\rangle$ is even at higher temperatures. Such an extreme crystal field splitting was also proposed for $CeRh_3B_2$ in Ref. 25.

C. Specific heat

The specific heat was studied for $0.0 \leqslant x \leqslant 0.6$ in the temperature region from 1.5 K up to about 150 K. The Rh-rich ferromagnetic compounds could only be used to determine the Sommerfeld value γ since the poor thermal contact between sample and the sample holder did not allow an unambiguous interpretation of the high-temperature part. However, the observation of distinct anomalies in $C_p/T(T)$ curves for the concentrations $0.125 \leqslant x \leqslant 0.3$ confirmed the

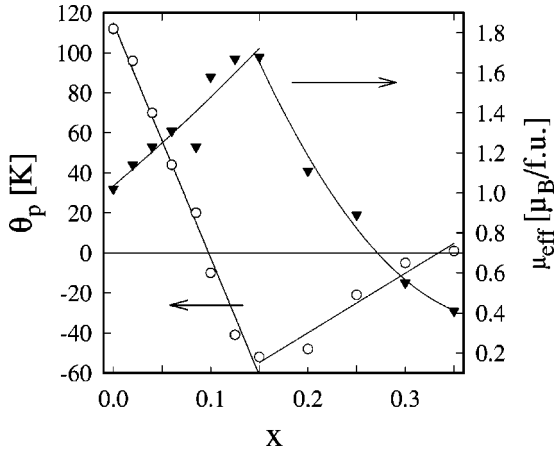

FIG. 7. Concentration-dependent paramagnetic Curie temperature θ_p, and effective magnetic moment μ_{eff} of $Ce(Rh_{1-x}Ru_x)_3B_2$.

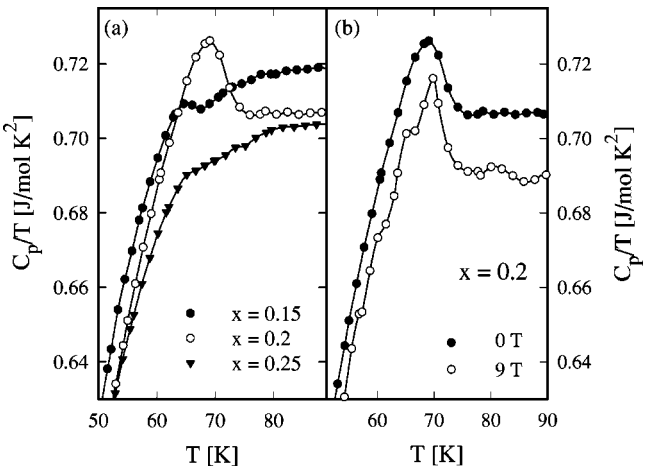

FIG. 8. (a) Temperature-dependent specific heat C_p of $Ce(Rh_{1-x}Ru_x)_3B_2$, $x=0.15,0.2,0.25$ plotted as C_p/T vs T. (b) Field-dependent specific heat C_p of $(CeRh_{0.8}Ru_{0.2})_3B_2$.

existence of long-range magnetic ordering as shown in Fig. 8(a). A field-dependent study of the specific heat up to 9 T did not reveal substantial changes of the ordering temperature [Fig. 8(b)]. The small effect of the magnetic field confirms the weakness of the ordered magnetic moments and its itinerant character in this concentration range. Thus, the interaction strength between moments has to be large to induce such high-temperature transitions. The strong magnetic exchange among the moments also points to an itinerant character of the system. Above $x=0.35$, hints for long-range magnetic order could not be retrieved due to the gradual transition into a paramagnetic regime.

The concentration-dependent variation of the γ values derived from extrapolations of $6<T<15$ K is shown in Fig. 9(a). The two characteristic maxima at $x=0.1$ and $x=0.4$ mark the intermediate regions between ferromagnetism and complex magnetic order ($x\approx0.1$) as well as between complex magnetic order and paramagnetic region ($x\approx0.4$). The enhanced γ values reflect the regions with a high degree of magnetic disorder. The additional data point at $x=0.4$, extracted from a low-temperature measurement ($T\geqslant0.4$ K), confirms the extrapolated values.

In order to determine the magnetic contribution to the specific heat as well as the magnetic entropy, we collected specific heat data for three isotypic La compounds $x=0,0.2,0.4$ in the temperature range 1.5 to 150 K. The γ values deduced from low-temperature extrapolations are 12, 13.5, and 5.3 mJ/mol K^2, respectively, in agreement to a recent study of Kasaya *et al.*[17] For $LaRh_3B_2$, the onset of superconductivity is clearly seen at $T\approx2.1$ K. It is worthwhile to note that a low-temperature evaluation ($T<10$ K) of the observed heat capacity data of the La alloys yielded large Debye temperatures $\Theta_D^{LT}=425$, 435, and 440 K for $x=0$, 0.2 and 0.4, respectively. However, on the basis of a pure Debye-type frequency distribution, the maxima in C_p/T vs T curves observed at 80 K already indicate a significantly lower value of $\Theta_D\approx250$ K, consistent with an analysis of the temperature-dependent resistivity based on the Bloch Grüneisen law ($\Theta_D^{\rho}\approx220$ K), which was applied up to 300 K. Such a strong variation of Θ_D with temperature at which it is evaluated reflects a complex phonon excitation spectrum.

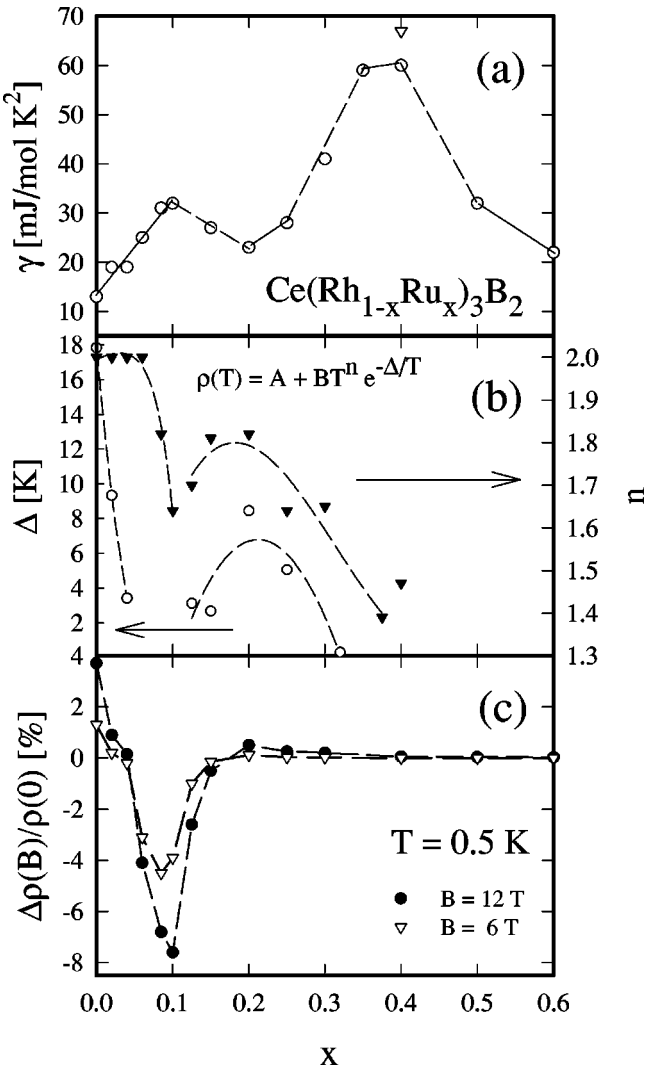

FIG. 9. Concentration dependence of (a) the Sommerfeld value γ (the single data point of γ for $x=0.4$ is taken from Ref. 14), (b) the energy gap Δ, and (c) the magnetoresistance $\Delta\rho/\rho$ obtained at $\mu_0H=6,12$ T and $T=0.5$ K.

It is of further interest that for Rh-rich compositions, at least up to $x=0.2$, the heat capacity of the La series between 10 and 40 K significantly surmounts that of the Ce compounds. This uncommon feature was already observed earlier by Shaheen *et al.*[26] and may be caused by Einstein type vibrations in the phonon spectrum which for the La case seem to excite at lower energies than for the Ce one. Thus a simple difference of the heat capacities between Ce and La compounds causes unphysical negative values. Therefore, in the case of $x=0.2$ we adopted a different approach, employing a model function consisting of a Debye base part in combination with a simple Einstein mode in order to fit the experimentally observed heat capacity data of the corresponding La-containing alloy. This fit was made to match the observed maximum in $C_p/T(T)$ as well as the high-temperature data,

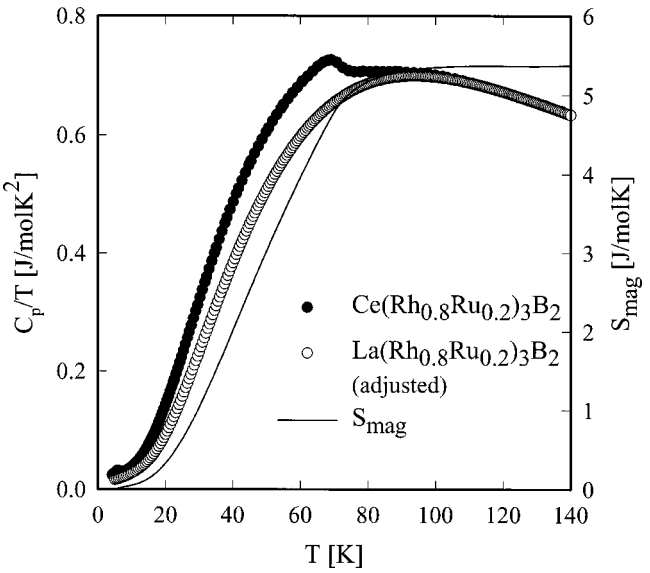

FIG. 10. Left axis: Temperature-dependent specific heat C_p of $Ce(Rh_{0.8}Ru_{0.2})_3B_2$ and of $La(Rh_{0.8}Ru_{0.2})_3B_2$ (adjusted, see text) plotted as C_p/T vs T. Right axis: Temperature-dependent magnetic entropy S_{mag} of $Ce(Rh_{0.8}Ru_{0.2})_3B_2$.

but with a small reduction in energies of the Einstein contribution in the low-temperature region (i.e., shifting the Einstein frequency to slightly higher temperatures). The shape of this function was adjusted to the observed maximum of the heat capacity data C_p/T vs T of the Ce alloy and then subtracted from the latter curve (see Fig. 10). The evaluation of the resulting curve finally yielded a magnetic entropy of $S_{mag} \approx 5.4$ J/mol K at 120 K, which is in fine agreement with a ground state doublet. For $x=0.4$ a direct subtraction of Ce and La experimental data yielding the magnetic contribution to the specific heat is acceptable and the magnetic entropy deduced amounts to roughly 4 J/mol K at 100 K. A Schottky-like evaluation of C_p, with a level splitting of about 500 K for the first excited level without accounting for possible hybridization is by far not able to produce such a high entropy. Rather, the formation of a nonmagnetic ground state would account for such an amount of entropy.

D. Electrical resistivity

The electrical resistivity of $Ce(Rh_{1-x}Ru_x)_3B_2$ is plotted in Figs. 11(a)–11(c). Due to easy formation of mechanical cracks during quenching, relative resistivities are given, normalized to 250 K. Pronounced extrema in the temperature derivatives of the resistivity data are only found in the region $0 \leqslant x \leqslant 0.06$. These extrema are taken as the transition into the ferromagnetically ordered state, well coinciding with the variation of T_C determined from Arrott plots. The broadening and blurring of such extrema in $d\rho/dT$ for compositions between $0.075 \leqslant x \leqslant 0.1$ is simply interpreted as the disappearance of long-range ferromagnetic order. Interestingly, extrema in $d\rho/dT$ again develop for the region $0.125 \leqslant x \leqslant 0.30$ indicative of the onset of a transition into long-range

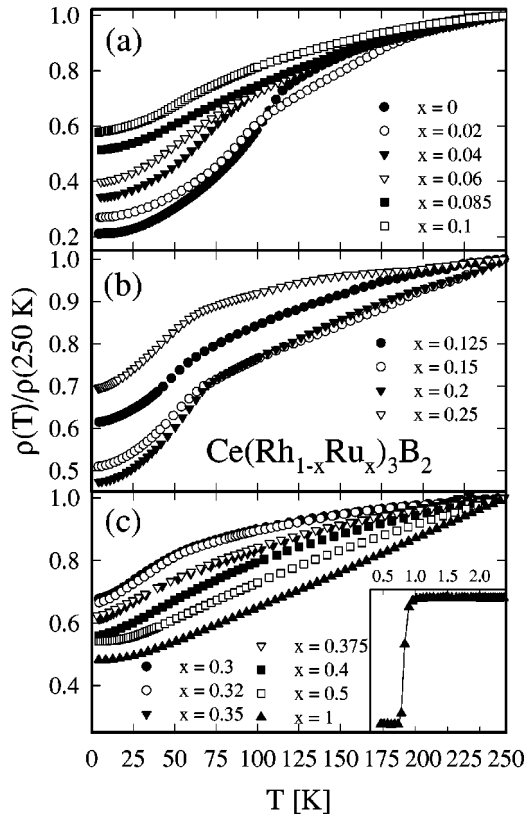

FIG. 11. (a)–(c) Temperature-dependent electrical resistivity ρ of $Ce(Rh_{1-x}Ru_x)_3B_2$ plotted in a normalized representation. The inset in (c) shows the onset of superconductivity of $CeRu_3B_2$.

magnetic order. These extrema become very small and finally die out for concentrations $x \geqslant 0.35$. It should be mentioned, however, that for the samples with $0.3 \leqslant x \leqslant 0.375$ the transition temperature does not approach zero indicating the prevalance of ''short-range-type'' magnetic order. The transition temperatures determined from electrical resistivity measurements are in good accord with the ordering temperatures derived from magnetic measurements and both sets of data were subsequently used to construct a magnetic phase diagram shown in Fig. 15.

In order to gain some insight into the major electron scattering mechanisms at low temperatures, we attempted to parameterize the experimental resistivity data with respect to

$$\rho = \rho_0 + AT^n \exp(-\Delta/T), \tag{1}$$

where ρ_0 represents the residual resistivity and Δ is the energy gap in the spin wave spectrum taking care of the strong anisotropy of this series. The contribution due to electron-phonon scattering at low temperatures was considered to be negligible. Figure 9(b) shows the parameters n and Δ obtained from least squares fits to Eq. (1) for a temperature region $T < (1/3)T_{C(N)}$. As preliminary refinements of the exponent n for the ferromagnetic region led to values close to $n=2$, we constrained the values for this region ($0.0 \leqslant x \leqslant 0.06$) to $n=2$. The quadratic power law is justified from

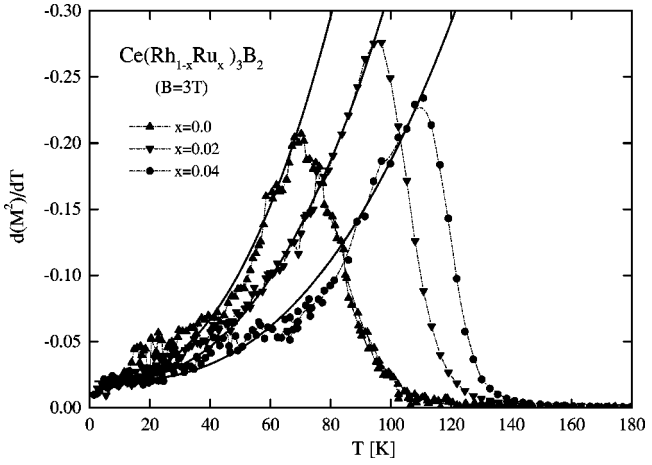

FIG. 12. Temperature dependence of $d(M^2)/dT$ of $Ce(Rh_{1-x}Ru_x)_3B_2$, $x=0.0, 0.02, 0.04$.

theoretical model calculation based on a ferromagnetic spin wave dispersion relation. The energy gap $\Delta=18$ K for $CeRh_3B_2$ decreases on Rh/Ru substitution and vanishes for $x=0.06$. For Ru concentrations $x>0.06$, the exponent n shows a minimum roughly at $x=0.1$ that is at a concentration where corresponding magnetic data show the breakdown of long-range ferromagnetic order. On further Rh/Ru substitution, a rising temperature exponent is concomitant with the reappearance of the energy gap both exhibiting peak values around $x=0.2$, where the ordering temperature of the complex magnetic phase finds its maximum. Finally, the drop of the magnetic ordering temperature for even higher Ru concentrations is accompanied by a simultaneous decrease of n to values around 1.5 and an approach of Δ towards zero. Values for the temperature exponent $n=3/2$ or 5/3 of the electrical resistivity are typical for a non-Fermi-liquid behavior in the vicinity of quantum critical point near a decaying two-dimensional or three-dimensional antiferromagnetic ordered state, respectively. Low-temperature specific heat measurements ($T\rightarrow 0.4$ K) on the sample $x=0.4$ already revealed significant deviations from a typical Fermi-liquid state.[15]

It is worthwhile to note that for ferromagnetic systems the derivative of the square of the spontaneous magnetization with respect to temperature represents the variation of the internal magnetic energy. In terms of thermodynamics, this quantity is the magnetic contribution to the specific heat. Figure 12 shows the corresponding set of data for the alloys $x=0.0$, 0.02, and 0.04. A satisfactory analytical description in terms of $d(M^2)/dT \propto C_{\mathrm{mag}}$ is obtained using the following expression:

$$C_{\mathrm{mag}}=BT^m\exp(-\Delta/T) \tag{2}$$

where B is a constant and the exponential function is expected in anisotropic systems with an energy gap Δ in the magnon spectrum. The values deduced for Δ as a function of composition decrease from 18 K to zero as ferromagnetic order vanishes, matching the dependence evaluated from the resistivity data. The exponent m is close to 3. Despite the fact that this is not the value expected for isotropic ferromagnets, model calculations of the spin wave contribution to the specific heat predict a value of $m=5/2$ for the moment lying in the basal plane,[27] which is evidenced for this compound from neutron elastic scattering.

E. Magnetoresistance

The field dependence of the electrical resistivity was measured for all concentrations at temperatures from 0.5 to 100 K and fields up to 12 T. Results are summarized in Fig. 9(c) plotting the magnetoresistance $[\rho(B)-\rho(0)]/\rho(0)$ for the Ce alloys up to $x=0.6$ for two different fields and $T=0.5$ K. As a general feature for this type of material, the overall value of $[\rho(B)-\rho(0)]/\rho(0)$ was found to be rather small. While the magnetoresistance for $x=0$ remains positive throughout the entire temperature range, small additions of Ru ($x=0.04$) reduce the magnetoresistance significantly to 0.4% at $T=0.5$ K, turning to a negative value of $-4\,\%$ at 0.5 K for $x=0.06$. In accordance with magnetization data, the alloy with $x=0.06$ may thus be considered to be at the borderline where long-range magnetic order commences to vanish. The minimum in magnetoresistance observed at around $x=0.08$ and $x=0.1$ (-7 and $-8\,\%$, respectively) then correlates with a maximum magnetic disorder in the alloys, marking the transition from the ferromagnetic regime towards the region with complex magnetic order also seen from magnetization and resistivity as well as from specific heat data. Although the magnetoresistance for $x=0.125$ and 0.15 is still slightly negative, there is a significant trend towards a positive magnetoresistance throughout the region of complex magnetic order $0.12\leqslant x\leqslant 0.4$.

The observation of a rather small positive magnetoresistance for both ordered regimes indicates a high molecular field with respect to the maximum applied field of 12 T. Hence the field dependency of the magnetoresistance in the investigated field region appears to be extremely small. Although the magnetoresistance for typical ferromagnets is negative, the positive value of the classical magnetoresistance may thus dominate. Statistical disorder due to the Rh/Ru substitution will decrease the classical magnetoresistance. This effect in combination with a still high molecular field present in the complex antiferromagnetic regime $0.12\leqslant x\leqslant 0.4$ yields the rather low positive magnetoresistance of $+0.5\,\%$ at 0.5 K as observed for $x=0.2$, where the magnetic ordering temperature assumes its maximum value ($T_N=67$ K).

F. High-temperature behavior

Shown in Fig. 13 are resistivity measurements of $Ce(Rh_{1-x}Ru_x)_3B_2$, $x\leqslant 0.4$, performed also above room temperature. $\rho(T)$ is normalized to each individual maximum value. Most interestingly, the resistivity of this series does not follow a simple metallic behavior at elevated temperatures. Rather, beyond some smooth maximum, the resistivity decreases upon further temperature rise. Moreover, the maximum in $\rho(T)$ shifts towards higher temperatures as the Ru content increases.

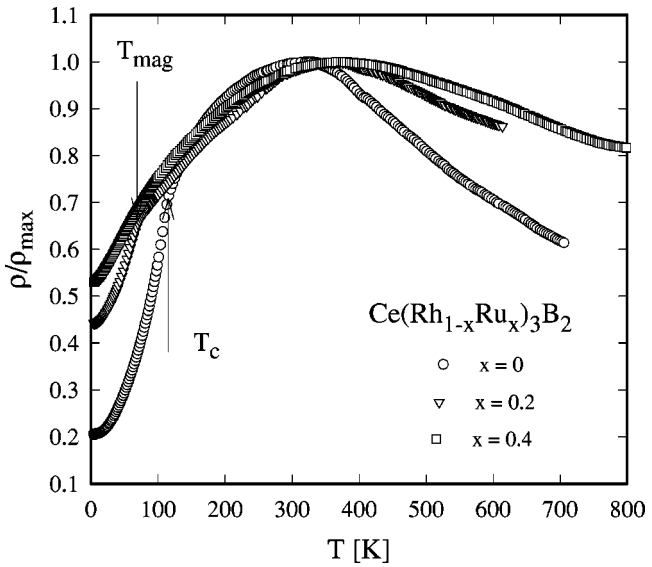

FIG. 13. Temperature-dependent electrical resistivity ρ of $Ce(Rh_{1-x}Ru_x)_3B_2$ ($x=0,0.2,0.4$), plotted in a normalized representation.

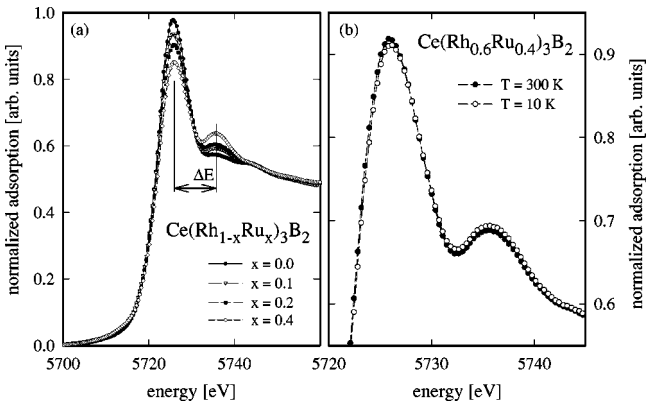

FIG. 14. (a) Energy dependence of the L_{III} absorption edge spectra of $Ce(Rh_{1-x}Ru_x)_3B_2$, $x=0,0.1,0.2,0.4$. (b) Energy dependence of the L_{III} absorption edge spectra of $Ce(Rh_{0.6}Ru_{0.4})_3B_2$ measured at $T=300$ K and $T=10$ K.

Several mechanisms are known, causing significant deviations of the electrical resistivity from typical metallic $\rho(T)$ features. Among them are (i) Kondo type interaction, yielding the famous $-\ln T$ law for temperatures above about the characteristic temperature T_K. (ii) Spin fluctuations, which are frequently observed in $f-d$ compounds such as RCo_2 ($R=$ rare earth). Such spin fluctuations can cause a steep increase of $\rho_{\mathrm{mag}}(T)$ at low temperatures, followed by decrease after a broad maximum (compare, e.g., Ref. 28). The latter occurs in that region where the magnetic susceptibility enters the high-temperature Curie-Weiss behavior of a spin fluctuation system. Additionally, the observed γ values of the specific heat of $Ce(Rh_{1-x}Ru_x)_3B_2$ would be compatible with a spin fluctuation concept. (iii) Localization of charge carriers due to disorder throughout the crystal. Many ternary, slightly off-stochiometric compounds exhibit at higher temperatures a negative coefficient of $\rho(T)$. Examples are, e.g., nonmagnetic compounds near the composition of YCu_4In.[29]

Concerning the ferromagnetism of the Rh-rich compounds, one may conclude that the resistivity behavior at high temperatures matches classical itinerant spin fluctuation systems rather than that of typical Kondo compounds. In this scenario, Ce $5d$ states would be responsible of forming magnetic states in the proximity of the Fermi energy. The importance of the Ce $5d$ magnetic states was already quoted in the introduction. In fact, this possibility is corroborated from our band calculations, revealing itinerant Ce $5d$ states below the Fermi energy. Classical spin fluctuation systems such as $ScCo_2$, YCo_2, or $LuCo_2$ do exhibit features as those discussed above.[28]

G. Absorption edge spectroscopy

Results of L_{III} XAS measurements at 300 K, performed on samples with $x=0$, 0.1, 0.2, and 0.4 are displayed in Fig. 14(a). In core level spectroscopies, such as XAS, it is well known that the high-energy structure with respect to the white line in the L_{III} absorption edge is a fingerprint of the $4f$-hybridization, and routinely used to estimate the $4f$ occupation in highly correlated systems. As shown in this figure, the white line centered at 5725 eV, decreases in intensity as the Ru doping is increased, whereas the high-energy structure, representing the "$4f^0$" state, strongly increases. Nevertheless, $CeRh_3B_2$ already exhibits a clear "$4f^0$" structure which is not observed in nonmagnetic isotypic $LaRh_3B_2$.[10] Though a quantitative evaluation is uncertain, the experimental results match those observed for the nonmagnetic compounds such as $CeRu_2Si_2$ or $CeBe_{13}$.[30] L_{III} measurements performed at $T=300$ K and $T=10$ K for samples rich in Rh reveal no experimentally resolvable temperature variation of the spectral intensities associated with the $4f^1$ and the $4f^0$ state. This fact introduces two possible scenarios, one with T_K smaller than the thermal energy window ($10<T<300$ K) and the other with $T_K>300$ K. The first possibility would be in agreement with magnetic order within a $4f$ localized picture, but with no confirmation from the temperature-dependent resistivity and in conflict with the extremely high T_C value. On the other hand, an itinerant description, with characteristic energy scales larger than room temperature, will allow one to match the four experimental facts, i.e., "$4f^0$" structure, temperature-independent L_{III} edges, the continuous increase of the electrical resistivity with temperature, and the high-T_C value. However, for the more Ru-concentrated alloys a small thermal variation of the spectral intensities is observed [compare Fig. 14(b) for $x=0.4$]. A closer inspection of Fig. 14(b) shows that the $4f^0$ spectral weight increases on the lowering of temperature, while the opposite occurs for $4f^1$. This particular behavior can be associated with an increase of hybridization, possibly due to the reduction of the unit cell volume on cooling. In fact, as it is obvious from Fig. 3 the specimen with $x=0.4$ is one where both lattice parameters a and c decrease with temperature.

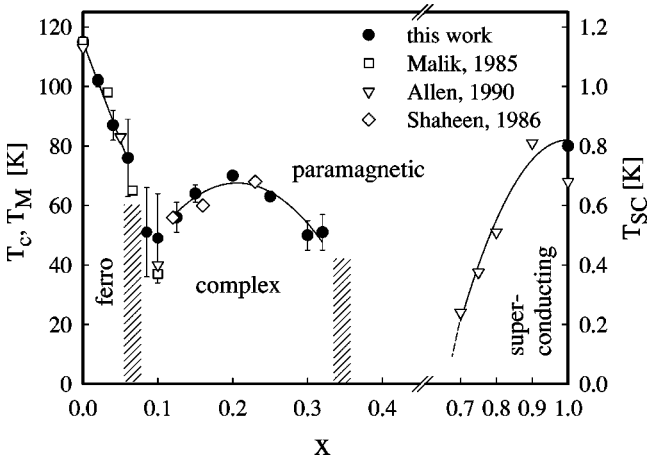

FIG. 15. Phase diagram of $Ce(Rh_{1-x}Ru_x)_3B_2$.

Concerning the evolution of the $4f$ occupation number n_f in $Ce(Rh,Ru)_3B_2$, the intensity of the reference structure of $4f^0$ is strongly affected by the Rh/Ru substitution [see Fig. 14(a)]. Indeed, only 10% of Ru increases the spectral weight of the $4f^0$ structure by a factor of 3. The energy separation of both spectral intensities does not change significantly upon the Rh/Ru substitution. Such a particular behavior was frequently observed in intermediate valence systems and even used to define the degree of hybridization of such compounds.[31]

Assuming a linear relationship between the $4f^1$ and $4f^0$ spectral intensities and the respective $4f$ electron count yields a decrease by a factor of about 1.3 when proceeding from $CeRh_3B_2$ to $Ce(Rh_{0.6}Ru_{0.4})_3B_2$. The increase of spectral weight of the $4f^0$ feature in the L_{III} data upon increasing Ru content implies a reduction of occupation of the magnetic state $4f^1$. However, the almost unchanged values of ΔE indicate that there occurs no substantial enhancement of hybridization of the $4f$ states. This is in fine agreement with the above band structure calculations where no significant changes of the $4f$ band width were derived when proceeding from Ru to Rh and Pd.

Moreover, the reduction of the mean $4f^1$ occupation would be in line with the initial decrease of T_C in the Rh-rich samples since the associated density of states involved in the Ruderman-Kittel-Kosuya-Yosida (RKKY) interaction will decrease accordingly, thereby reducing the ordering temperature. This is not in conflict with the observed initial increase of the effective magnetic moment, where the more localized character due to an increasing Ce-Ce distance plays a major role.

H. Phase diagram

The results of magnetic, thermal, and transport measurements are summarized in Fig. 15, including previous results[15,16] and the formation of a superconducting state on the Ru-rich side.[13] The phase diagram of $Ce(Rh_{1-x}Ru_x)_3B_2$ presents four different regimes: ferromagnetism $0 \leqslant x \leqslant 0.06$, with T_c dropping from 115 K to about 50 K at $x = 0.06$, next to a region of complex magnetic order for $0.12 \leqslant x \leqslant 0.32$ where magnetic ordering temperatures exhibit a shallow maximum $T_m = 67$ K at about $x = 0.20$, followed by a paramagnetic region for $x \geqslant 0.40$. Finally, superconductivity sets in for $x \geqslant 0.7$.

The ferromagnetic phase observed at the Rh-rich side is replaced by a complex magnetic phase of antiferromagnetic character after crossing through a magnetically disordered regime within $0.08 \leqslant x \leqslant 0.12$. A coherent magnetic ground state is fully recovered around $x = 0.2$ as evidenced by the well defined specific heat jump at $T_m = 67$ K. The nonmagnetic region, showing the characteristics of intermediate valent behavior, is reached when the effective magnetic moment extrapolates to zero at about $x \approx 0.4$. This coincides with a loss of the features in $\chi(T)$, $C_p(T)$, and $\rho(T)$ associated with the complex AFM order. Contrary to the ferromagnetic to complex phase transition, the vanishing of effective magnetic moments at concentrations $x \approx 0.4$ excludes the possibility of a first order phase transition into the nonmagnetic phase. Nevertheless distinct deviations from a Fermi-liquid behavior are observed from the low value ($n \approx 1.4$) of the exponent in the temperature-dependent resistivity.

IV. SUMMARY

The experimental results presented here confirm the fact that the alloy series $Ce(Rh_{1-x}Ru_x)_3B_2$ cannot be treated as a typical Kondo-lattice system. Not only does the extremely high ordering temperature of $CeRh_3B_2$ stick out from a localized $4f$-electron description, but also its ferromagnetic character and the extremely short Ce-Ce spacings require a new microscopical description with respect to the competition among classical Kondo versus RKKY interactions.[32]

The obtained magnetic phase diagram shows a drastic drop of the ordering temperature at low Ru concentration (about 6 K/at. % Ru) which does not pass over directly into a nonmagnetic phase. On the contrary, a magnetic phase sets in, still exhibiting remarkably high ordering temperatures but being weakly concentration dependent. This change of magnetic structure indicates a strong modification of the magnetic interaction, but confirms the persistence of magnetic moments. The discontinuity of its paramagnetic phase boundary at the edge to the nonmagnetic phase also indicates the peculiar ground state properties of the system at hand.

The loss of the mean $4f^1$ population upon Rh/Ru substitution without a significant increase of the hybridization explains the initial decrease of T_C as well as the growing importance of the Ce $5d$ states, dominating the magnetic behavior and shifting the system towards a more and more itinerant d-band system. There, large ordering temperatures are conceivable and by no means contradict even very small ordered moments.

ACKNOWLEDGMENTS

This work was supported by Austrian Grant Nos. FWF P13544 and P12899 as well as by the Argentinian CONICET, Project No. 811.

[1] S.K. Dhar, S.K. Malik, and R. Vijayaraghavan, J. Phys. C **14**, L231 (1981).
[2] K.N. Yang, M.S. Torikachvili, M.B. Maple, and H.C. Ku, J. Low Temp. Phys. **56**, 601 (1984).
[3] B. Maple, S.E. Lambert, M.S. Torikachvili, K.N. Yang, J.W. Allen, B.B. Pate, and L. Lindau, J. Less-Common Met. **111**, 239 (1985).
[4] S.A. Shaheen, J.S. Schilling, and R.N. Shelton, Phys. Rev. B **31**, 656 (1985).
[5] K. Takegahara, H. Harima, and T. Kasuya, J. Phys. Soc. Jpn. **54**, 4743 (1985).
[6] T. Kasuya, M. Kasaya, K. Takegahara, F. Iga, B. Liu, and N. Kobayashi, J. Less-Common Met. **127**, 337 (1987).
[7] T. Kasuya, K. Takegahari, N. Kobayashi, M. Kasaya, and A. Okabe, in *Theoretical and Experimental Aspects of Valence Fluctuations and Heavy Fermions*, edited by L.C. Gupta and S.K. Malik (Plenum, New York, 1987), p. 187.
[8] S.K. Malik, A.M. Umarji, G.K. Shenoy, P.A. Montano, and M.E. Reeves, Phys. Rev. B **31**, 4728 (1985).
[9] J.A. Alonso, J.X. Boucherle, F. Givord, J. Schweizer, B. Gillon, and P. Lejay, J. Magn. Magn. Mater. **177-181**, 1048 (1998).
[10] E.V. Sampathkumaran, G. Kaindl, C. Laubschat, W. Krone, and G. Wortmann, Phys. Rev. B **31**, 3185 (1985).
[11] A. Fujimori, T. Takahashi, A. Okabe, M. Kasaya, and T. Kasuya, Phys. Rev. B **41**, 6783 (1990).
[12] A. Yaouanc, P. Dalmas de Reotier, J.-P. Sanchez, Th. Tschentscher, and P. Lejay, Phys. Rev. B **57**, R681 (1998).
[13] J.W. Allen, M.B. Maple, J.-S. Kang, K.N. Yang, M.S. Torikachvili, Y. Lassailly, W.P. Ellis, B.B. Pate, and I. Lindau, Phys. Rev. B **41**, 9013 (1990).
[14] S.K. Malik, A.M. Umarji, G.K. Shenoy, and M.E. Reeves, Solid State Commun. **54**, 761 (1985).
[15] E. Bauer, R. Hauser, A. Galatanu, A. Lindbaum, G. Hilscher, H. Sassik, H. Kirchmayr, J.G. Sereni, and P. Rogl, J. Appl. Phys. **83**, 6423 (1998).
[16] St. Berger, R. Hauser, H. Michor, G. Hilscher, E. Bauer, J.G. Sereni, and P. Rogl, Physica B **259-261**, 116 (1999).
[17] M. Kasaya, Y. Abe, J.L. Li, and T. Kasuya, Physica B **163**, 317 (1990).
[18] J. Langen, G. Jackel, W. Schlabitz, M. Veit, and D. Wohlleben, Solid State Commun. **64**, 169 (1987).
[19] D. C. Koskenmaki and K.A. Gschneidner, Jr., in *Handbook on the Physics and Chemistry of Rare Earths*, edited by K. A. Gschneidner, Jr. and L. Eyring (Elsevier Science, Amsterdam, 1978), Vol. 1, p. 337.
[20] A.R. Williams, J. Kübler, and C.D. Gelatt, Jr., Phys. Rev. B **19**, 6094 (1979); V. Eyert, Int. J. Quantum Chem. **77**, 1007 (2000) (for a recent review).
[21] D.D. Koelling and B.N. Harmon, J. Phys. C **10**, 3107 (1977).
[22] J. von Barth and D. Hedin, J. Phys. C **5**, 1629 (1972).
[23] J.F. Janak, Solid State Commun. **25**, 53 (1978).
[24] M. Kasaya, A. Okabe, T. Takahashi, T. Satoh, and T. Kasuya, J. Magn. Magn. Mater. **76-77**, 347 (1988).
[25] K. Yamaguchi, H. Namatame, A. Fujimori, T. Koide, T. Shidara, M. Nakamura, A. Misu, H. Fukutani, M. Yuri, M. Kasaya, H. Suzuki, and T. Kasuya, Phys. Rev. B **51**, 13 952 (1995).
[26] S.A. Shaheen, J.S. Schilling, and R.N. Shelton, J. Magn. Magn. Mater. **54-57**, 357 (1986).
[27] A. I. Akhiezer, V. G. Bar'yakhtar, and S. V. Peletminskii, in *Spin Waves*, edited S. Doniach (North-Holland, Amsterdam, 1968), Chap. 6.
[28] E. Gratz, R. Resel, A.T. Burkov, E. Bauer, A.S. Markosyan, and A. Galatanu, J. Phys.: Condens. Matter **7**, 6687 (1995).
[29] E. Bauer, M. Forsthuber, R. Hauser, G. Hilscher, T. Holubar, R. Resel, and G. Schaudy, Physica B **194-196**, 1163 (1994).
[30] D. Wohlleben and J. Rohler, J. Appl. Phys. **55**, 1904 (1984).
[31] J. Rohler, J. Magn. Magn. Mater. **47-48**, 175 (1985).
[32] S. Doniach, Physica B **91**, 37 (1977).